Geometrical equilibrium of curves: a showcase of helical numerical solutions



2004 J. Phys. A: Math. Gen. 37 9419

(http://iopscience.iop.org/0305-4470/37/40/007)

INSTITUTE OF PHYSICS PUBLISHING JOURNAL OF PHYSICS A: MATHEMATICAL AND GENERAL

J. Phys. A: Math. Gen. **37** (2004) 9419–9438 PII: S0305-4470(04)79809-1

# Geometrical equilibrium of curves: a showcase of helical numerical solutions

**Guillermo Arreaga-García, Hugo Villegas-Brena and Julio Saucedo-Morales**

Centro de Investigación en Física de la Universidad de Sonora, Apdo. Postal 14740, CP. 83000, Hermosillo, Sonora, Mexico

E-mail: garreaga@cajeme.cifus.uson.mx

Received 23 April 2004, in final form 20 August 2004
Published 22 September 2004
Online at stacks.iop.org/JPhysA/37/9419
doi:10.1088/0305-4470/37/40/007

**Abstract**

In this work we plot loop configurations that minimize energy functionals depending on geometrical invariants of the loop itself. In particular, we consider a family of functionals including curvature and torsion terms, both linear and quadratic, such that their combinations produce geometrical invariants. In [1], Noether's theorem was advantageously used to identify the constants of integration of the Euler–Lagrange equations describing the equilibrium of loops for this family of energy functionals. Those authors demonstrated the integrability of these functionals by means of quadratures. In this work we follow that approach to realize numeric calculations and to show plots of numerical solutions of the relevant equations for equilibrium of loops, as these were presented but not studied in [1]. We then show as the main result of this work a representative catalogue of such solutions in Euclidean three-dimensional space.

PACS numbers: 02.30.Xx, 11.10.Ef, 61.41.+e

## 1. Introduction

Let us consider a curve $\mathbf{X}(s)$ embedded in an Euclidean three-dimensional space, such that $s$ is an arbitrary parameter and $l$ is the arc length:

$$l(s) = \int_0^s \mathrm{d}s' \sqrt{\frac{\mathrm{d}\mathbf{X}}{\mathrm{d}s'}\frac{\mathrm{d}\mathbf{X}}{\mathrm{d}s'}}. \tag{1.1}$$

The unit tangent vector is defined as[1] $\mathbf{t} = \frac{\mathrm{d}\mathbf{X}}{\mathrm{d}l}$. If the curve is smooth enough everywhere, it will always be possible to define a Frenet–Serret vector basis at each point $(\mathbf{t}, \mathbf{n}_1, \mathbf{n}_2)$, where

[1] In what follows, a prime will denote derivative with respect to $l$, so that $\mathbf{t} \equiv \mathbf{X}'$.

  

$\mathbf{n}_1$ and $\mathbf{n}_2$ are the normal and binormal vectors, respectively. The evolution of these vectors along the curve will be described by the classical Frenet–Serret equations

$$\begin{aligned} \mathbf{t}' &= \kappa \mathbf{n}_1 \\ \mathbf{n}_1' &= -\kappa \mathbf{t} + \tau \mathbf{n}_2 \\ \mathbf{n}_2' &= -\tau \mathbf{n}_1. \end{aligned} \tag{1.2}$$

where $\kappa(l)$ and $\tau(l)$ are the curvature and torsion of the curve, respectively; additionally, an orientation $\mathbf{n}_2 = \mathbf{t} \times \mathbf{n}_1$ is chosen, see [2].

Let us associate with the curve an energy that depends on its configuration through its curvature and torsion. The most general energy functional one can write has the form:

$$H[\mathbf{X}] = \int \mathrm{d}l \, f(\kappa, \tau), \tag{1.3}$$

where $f(\kappa, \tau)$ must be invariant under coordinate changes of the background space and under transformations of the generating parameter $l$. Some examples of functionals satisfying these requirements are: $(i) f = \mathbf{t}' \cdot \mathbf{t}' = \kappa^2$, $(ii) f = \mathbf{n}_1' \cdot \mathbf{n}_1' = \kappa^2 + \tau^2$ and $(iii) f = \mathbf{n}_2' \cdot \mathbf{n}_2' = \tau^2$.

When $f$ depends quadratically on $\kappa$ or $\tau$ only, for instance $f(\kappa) = \kappa^2$ or $f(\tau) = \tau^2$, some curves that minimize $H$ are known for a long time to be helices (for a pedagogical review, see [3] and references therein). This fact motivated some authors to look for a physical application of these kind of theories as they considered this helix to be the ground-state conformation of a chiral polymer [4]. For instance, let us mention the mechanical elastic model for the double chain of DNA molecule which was proposed in the eighties, see [5] and references therein. This model is based on the hypothesis that for large length scales compared to the range of the molecular interaction between the chain and its environment, the duplex DNA has the mechanical properties of a symmetric, linearly elastic rod and therefore it responds to the environment in the same way that a stiff rod does under loads in material science, see [6]. This mechanical picture is known to be useful for representing DNA equilibrium states, as well as the occurrence of supercoiling [7]. Then the primary assumption of this elastic model would be that the loop (rod) has an elastic energy $H$ composed of two parts: the bending energy $H_b$ and the torsional energy $H_t$

$$H[\mathbf{X}] = H_b + H_t \equiv \int \mathrm{d}l \frac{A}{2}(\kappa - \kappa_0)^2 + \int \mathrm{d}l \frac{C}{2}(\tau - \tau_0)^2, \tag{1.4}$$

where $A$ and $C$ are the bending and torsional stiffness coefficients, respectively, see [8].

Even for simpler forms of $f$ than that proposed in equation (1.4), the resulting field theory is quite involved due to the complex dependency of $\kappa$ and $\tau$ on $\mathbf{X}$ so that a qualitative understanding of the solutions is hard to achieve. In spite of the physical motivation, as far as we know, not much work has been devoted to finding equilibrium configurations of curves for functionals like that of equation (1.4) in the most general case—even though there is in fact already a tradition of using an Euler-angles approach to find exact solutions in terms of elliptic integrals. See for instance, the work of Wadati [8]. Wadati shows the equilibrium configurations associated with a purely quadratic functional like that given in equation (1.4), obtained by considering elliptic integrals, but since such integrals can be solved analytically just for the simplest cases, these curves were limited to a plane. Therefore, it is our opinion that a global picture of all the possible geometric equilibrium shapes of curves still remains to be achieved, above all for energy functionals involving torsion, where little appears to be known.

On the other hand, models depending only on the curvature, $f = f(\kappa)$, have been known to be integrated by quadratures for some time (see [10]). In fact, and from a purely algebraic point of view, the resulting quadratures are analogous to those arising in the problem of a

particle moving in a central potential, with the roles of time and spatial coordinates replaced by the arc length and curvature, respectively.

Recently, taking advantage of this approach of integration by quadratures, Arreaga, Capovilla, Chyssomalakos and Guven considered, in [11], the case of a functional that depends quadratically on the curvature, for a closed loop on the plane such that its equilibrium configurations have two constraints, one on its total length, the other on the total area enclosed by the loop. The energy functional they considered was:

$$H = \alpha \int \mathrm{d}l\, \kappa^2 - \mu \left( \int \mathrm{d}l - L \right) + \sigma \left( \int \mathrm{d}^2 x - A \right). \tag{1.5}$$

They showed that a complete analysis of such a model with three parameters, $(\alpha, \mu, \sigma)$, is far from trivial. The analysis of the function corresponding to the effective potential in this case was complicated, and it was then necessary to resort to numerical techniques in order to integrate the field equations. However, the richness of the types of solutions was clear: some curves were found to be self-intersecting, others were not, but in either case, they had a high degree of symmetry and geometric appeal (see for instance figures 8 and 9 in [11] and chapter 4 of [12] as well). Additionally, if one inspects the wide range of solutions obtained, it can be noted that some of them resemble the configurations observed among amphiphillic membranes. We recall that there is solid evidence that a curvature-depending functional, that proposed by Helfrich, captures the most relevant aspects of amphiphilic membrane configurations in thermal equilibrium for two-dimensional surfaces embedded in an Euclidean space, see [15].

In this paper we carry out a simple and straightforward extension of the work presented in [11], as we consider models with terms quadratic and linear on both the curvature and the torsion, so that families with several free parameters can be studied. We show a wide number of curves that are representative solutions to different energy functionals, including loops both on the plane and in an Euclidean three-dimensional space.

The integrability by quadratures of the models we have considered in this paper was already established by Capovilla, Chryssomalakos and Guven in [1]. They employed a general formalism based on exploiting Noether's theorem to identify the constant of integration of the Euler–Lagrange equations as the Casimirs of the Euclidean group in three dimensions. The integral associated with rotational invariance permits them to obtain a formula relating the torsion and the curvature in such a way that one of them can be expressed in terms of the other. The integral associated with translational invariance can then be cast as a quadrature for $\kappa$ or for $\tau$.

The integration by quadratures of functionals depending quadratically on the curvature was shown to be possible, as was previously known. Nevertheless, Capovilla, Chryssomalakos and Guven have also shown that the same approach holds true for functionals quadratic on the torsion, which is rather surprising given the nature of the field equations.

The formalism will not be reproduced here, rather, we shall focus our attention on the numerical solutions to be obtained, and the field equations will be shown only as needed. For further details the reader is directed to [1].

In this approach, the space curve configurations become as we sweep out the levels of the well of the effective potential starting from its minimum value. In this point, this approach offers differences with respect to the work about elastic filaments done by Nizette and Goriely in [16]. Indeed, taking advantage of the connection between the equations describing the statics equilibrium of rods and the dynamics of spinning tops, these authors have made a very interesting and complete classification of the 3D solution curves for the Euler–Kirchhoff elasticity model.

In spite of the interest of these kind of energy functionals as, among other things, mechanical models for polymer chains and for modelling the DNA supercoiled configurations (see [20–23]), we are not aware of any systematic study of the solutions or their properties other than the simplest configurations for the quadratic model in the curvature, as was shown in [5]. We insist that it remains to be seen what other types of solutions can be admitted by different models.

In this paper, we will plot solution curves for more functionals other than the pure curvature model, however, we postpone for a second part of this work, the problem to undertake an exhaustive classification of the solution curves from a geometrical point of view (see for instance [18] for the elastic rods). Rather, we will study the effective potential in order to obtain the solution curves. In the case of pure torsion models, as far as we know, this analysis is presented here for the first time. Then we will show a small number of curves in order to illustrate the geometrical nature of the solution family.

We will complete this project in a subsequent publication, where we will consider the response of these loops to shear flow. Then, in view of this new and more complete showcase of solutions curves, we will be in a position to consider the applicability of these energy models as mechanical toy models for representing some DNA physics.

This section has introduced some basic geometrical notions which allows us to properly state the geometric basis of these models. The rest of the paper is divided as follows: in section 2 we present solutions to the quadratic-curvature model, while section 3 deals with a simple extension that includes a linear term on the torsion; section 4 presents solutions for a purely quadratic model on the torsion and section 5 treats the corresponding extension to include a term linear on the curvature. Finally, section 6 presents some general comments on our results. Details of the numerical implementation can be found in the appendix.

## 2. Model I: $f(\kappa) = (\kappa - \kappa_0)^2 + \mu$

The purely quadratic-curvature model has been studied by mathematicians (see for instance [10, 13] and especially the work of Langer and Singer [14] who have obtained analytically the solution for this model in terms of elliptic integrals and have parametrized the space of solution of elastic curves by a triangular region of the parameter plane: they found that the solution curves are either closed curves or wind densely around a torus of revolution; they also found that closed curves form a countable set of points lying on a single curve within a triangle); by physicists in different contexts, among them, in special relativity (see [19] and references therein); in soft materials; and in polymer science (see [3]).

In [11] it was shown that plane curve solutions to the purely quadratic theory are much more interesting when one considers constraints both on the area and on the form of the curve on the energy functional simultaneously, see equation (1.5). In this way, the free parameters $(\mu, \sigma)$, together with the integration constant $E$ resulting from the quadrature, give a three-parameter solution space, which complicates the analysis of the effective potential associated with the quadrature. The problem of the elastica in the plane was also considered independently by Yang-Chan and Xing in [12].

This section considers the 3D generalization of the loops studied in [11] with an additional constant $\kappa_0$, which is introduced as a one-dimensional analogy to the spontaneous curvature of amphiphillic membranes (see [15]). However, here we do not enforce a constraint on the area enclosed by the curve, nor ask for the curve to be closed, since in general, the solutions for this model are open curves.

We mention that Nizette and Goriely have recently published a classification of the solution curves for the Euler–Kirchhoff filament model, see [16] and references therein. It

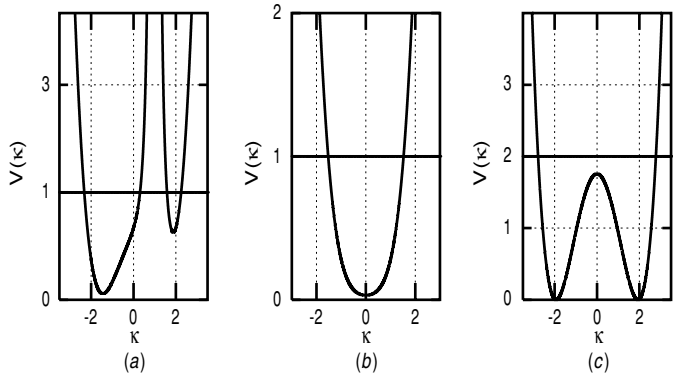


**Figure 1.** Effective potential $V(\kappa)$ for model I, for different values of $\mu$, $\kappa_0$ and $J$: (*a*) $\mu = \kappa_0 = J = 1.0$; (*b*) $\mu = -1.5,\ \kappa_0 = 1.0,\ J = 0$ and (*c*) $\mu = 1.5,\ \kappa_0 = 1.5,\ J = 0$.

would be worthwhile to follow this classification frame to undertake the same classification of the solution curves for the purely quadratic curvature model.

Following [1], the solution configurations for

$$f(\kappa) = (\kappa - \kappa_0)^2 + \mu \tag{2.1}$$

are determined by the differential equation:

$$2\kappa'' + \kappa^3 - \mu\kappa - \kappa\kappa_0^2 - \frac{2J^2}{(\kappa - \kappa_0)^3} = 0, \tag{2.2}$$

where $J$ is an integration constant that relates curvature and torsion:

$$\tau(\kappa) = \frac{J}{(\kappa - \kappa_0)^2}. \tag{2.3}$$

Equation (2.2) can be integrated by a quadrature as follows:

$$\tfrac{1}{2}\kappa'^2 + V(\kappa) = E, \tag{2.4}$$

where $E$ is a second integration constant and the effective potential $V$ is given by:

$$V(\kappa) = \frac{1}{8}\left(\kappa^2 - \kappa_0^2 - \mu\right)^2 + \frac{J^2}{2(\kappa - \kappa_0)^2}. \tag{2.5}$$

The structure of $V(\kappa)$ obviously depends on the value of the parameters $\mu$, $\kappa_0$ and $J$. Figure 1 shows the three kinds of configurations that can be obtained for $V(\kappa)$. It turns out that only the first case gives rise to curves in three dimensions, while the other two, having $J = 0$, produce curves contained on a plane. Horizontal lines with different values of $E$ allow to label each solution curve of the family.

Let us first consider solutions for graph (*a*), figure 1. The potential has two branches, each with a minimum, $V = V_{\min}$. Let us consider that $E = V_{\min}$ on either branch, then $\kappa$ and $\tau$ are constant and nonzero, let us say $\kappa = \kappa_{\min}$ and $\tau = \tau_{\min}$; and the solution curve is a helix with constants $a$ and $b$ as depending on $\kappa_{\min}$ and $\tau_{\min}$ as given in the appendix. These values of $\kappa_{\min}$ are obtained as roots of a six order polynomial in $\kappa$ whose solutions depend also on the values of $(\mu, \kappa_0, J)$.

For every value of $\mu$, whether positive or negative, as large as desired, there always are two real solutions for the six order polynomial and the behaviour of the critical curvature $\kappa_{\min}$ with $\mu$ is almost the same, irrespective of whether the value of $\kappa_0$ is zero or not. As $\mu$ takes

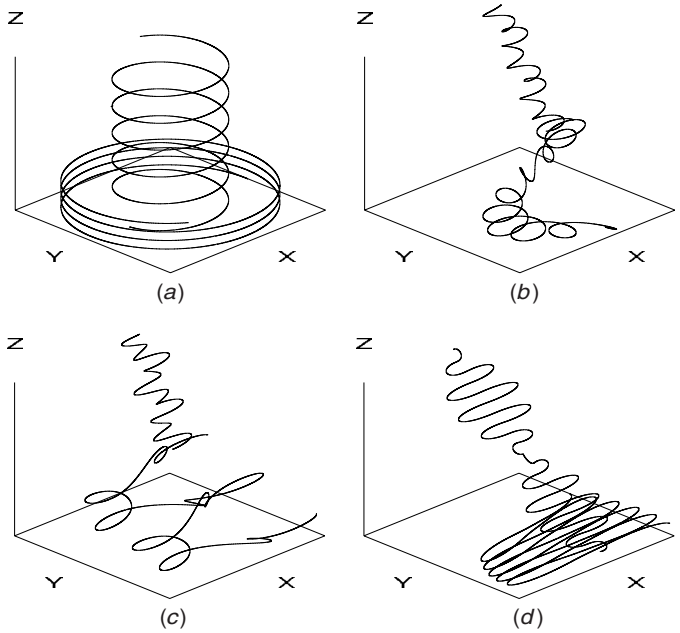


**Figure 2.** Solution curves for model I with $\mu = \kappa_0 = J = 1.0$, for different values of $E$: (*a*) $E = 0.0846\,(E = 0.9399)$, (*b*) $E = 0.431\,29\,(E = 1.0981)$, (*c*) $E = 0.7780\,(E = 1.2562)$, (*d*) $E = 1.1247(E = 1.4144)$, where the first (second) value corresponds to the left (right) branch of potential of figure 5 and to the bold (light) line, respectively.

the values of, for instance the interval $(-10, 10)$, starting from the negatives ones, the two branches are moving downward in the plane $V$ versus $\kappa$ from $V \approx (\kappa^2 - |\mu|)^2$ with $\kappa_{\min}$ almost constant $\kappa_{\min} \approx \left(\frac{2J}{\mu}\right)^{\frac{1}{4}}$. When $\mu$ reaches the value $\mu_p \approx -\kappa_0$, both branches start moving away from the asymptotically vertical line at $\kappa = \kappa_0$ and in such a case the value $\kappa_{\min} \approx \pm\sqrt{\mu}$ moves to the left (for left branch) and to the right (for right branch) in the plane $V$ versus $\kappa$.

Because the helix is the most prominent solution of this kind of energy functionals, it is worth following the geometric change of the helix as depending on the value of the parameter $\mu$ for model I. In fact, in figure 11 we show the behaviour of the ratio of the curvatures $\alpha = \frac{\kappa}{\tau}$ for the helix for each branch of the effective potential $V(\kappa)$ against $\mu$ for different models. What these curves indicate (see appendix) for model I is that the helices for each branch keep their diameter almost constant for $\mu \ll -\kappa_0^2$; when $\mu \gg -\kappa_0^2$, then the diameter (of the helices) starts increasing as $\mu$ increases. The difference between the helices for left and right branches found in model I is only the starting point of progress of the helix as long as they are both counterclockwise curves. We note also that the behaviour of the curves of figure 11 is qualitatively the same irrespective of the value of $\kappa_0$ for model I.

Now we try to describe the appearance sequence of the solution curves for model I as we inspect the values of the parameter $E$ in the potential well. For both branches of the potential, the initial cylindrical helix is notably geometrically distorted for values of $E$ very close to the minimum value. There appear loops, and the curve gets wounded in space. However, for large values of $E \gg E_{\min}$, symmetry of the curves is restored, but in this time, the curve forms an eight: simply in going to and getting back from its extreme points. The detailed way in which curves undergo this process is quite different for each branch of the potential. Such differences can be appreciated in figure 2 where we show three-dimensional solution curves

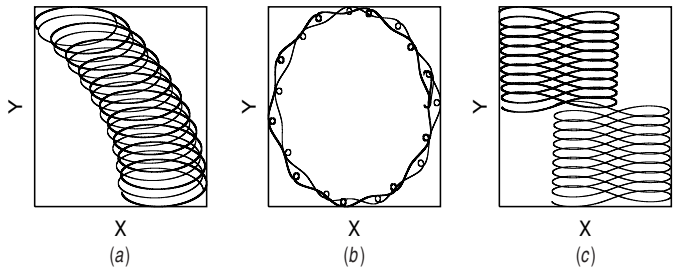


**Figure 3.** Solutions for case (*c*) of figure 1, model I. We show solutions with (*a*) $E = 0.5000$, (*b*) $E = 1.7577$ and (*c*) $E = 3.5000$, for both the left (solid line) and right (dotted line) branch of $V$.

to the Frenet–Serret equations (1.2) for this model. It is worth mentioning that curves here found for the left branch are reminiscent of the curves shown in figure 2 of [5].

Consider now solutions for panels (*b*) and (*c*) of figure 1, for which $J = 0$. In both cases, $V$ is symmetric under a reflection $\kappa \to -\kappa$, so that when $\mu + \kappa_0^2 \leqslant 0$, there is only one minimum, while for $\mu + \kappa_0^2 > 0$, $V$ has a maximum between the minima. The curves found for case (*b*) are uninteresting, as they only oscillate between their extrema. For case (*c*) there are two different types of curves, depending on whether $V_{\min} < E < V_{\max}$, or $E \gg V_{\max}$, see figure 3. In figure 3 we note that curves (*a*) and (*b*) belong to the same type, but whereas curve (*a*) is obtained for $E$ near $V_{\min}$, curve (*b*) corresponds to a value of $E$ near $V_{\max}$. Varying $E$ within the interval $V_{\min} < E < V_{\max}$, we can observe the circle generated for $E = V_{\min}$, turning into a series of elliptical loops winding around a bigger circle. As $E$ grows, the initial curvature tends to 0, so that the loop tends to consist of less curved segments, as can be seen in graph (*a*) of the same figure 3. Note also that the curves for both branches are essentially the same. In this case, the only closed curves are the circle and the figure eight, as was anticipated in [1]. Solutions like those shown in panel (*b*) of figure 3 are obviously more difficult to predict only on analytical grounds. One can take advantage of the fact that the value for $E$ for this solution is close to $V_{\max}$, in order to consider a perturbation analysis, and after that an analysis of stability for these kind of solutions would also be interesting.

Here $\kappa_0$ represents the tendency of the curve to be naturally not straight, that is, the lowest energy configuration is not a straight line. In our case, however, we do not find an important effect of $\kappa_0$ on the form of $V$. In particular, setting $\kappa_0 = 0$ only causes the graph (*a*) of figure 1 to become symmetric under the reflection $\kappa \to -\kappa$, while graphs (*b*) and (*c*) remain essentially the same, with $\mu$ determining entirely the form of $V$: $V$ has only one critical point for $\mu > 0$, but it has three critical points for $\mu < 0$. Figure 4 shows solutions for $\kappa_0 = 0$, with the same values of $E$ used to generate the curves in figure 2 in order to compare between them. It can be seen that they look less wound than is the case with $\kappa_0 \neq 0$.

To end this section, we plot in figure 5, the energy $H$ against $E$ for each curve with the parameters $\mu$,$J$ and $\kappa_0$ fixed to the values given in figure 1 for $V(\kappa)$. We note first that $E$ has no known physical meaning; it is just a label for the curves of the family and therefore, the plot is only meant to suggest a comparison between the different geometric structures of the curves in the family. Besides, according to equation (1.3), the value of $H$ depends on the total length of the curve, and in order to account only for geometric differences between the curves, we have then fixed the length of each curve to the same (arbitrary) value, say $L_0$. Additionally, we have integrated out the $\mu$ term in the calculation of $H$, since $\mu$ is introduced as a Lagrange multiplier for the constraint imposed on the total length of the curve, and not as a part of the energy itself.

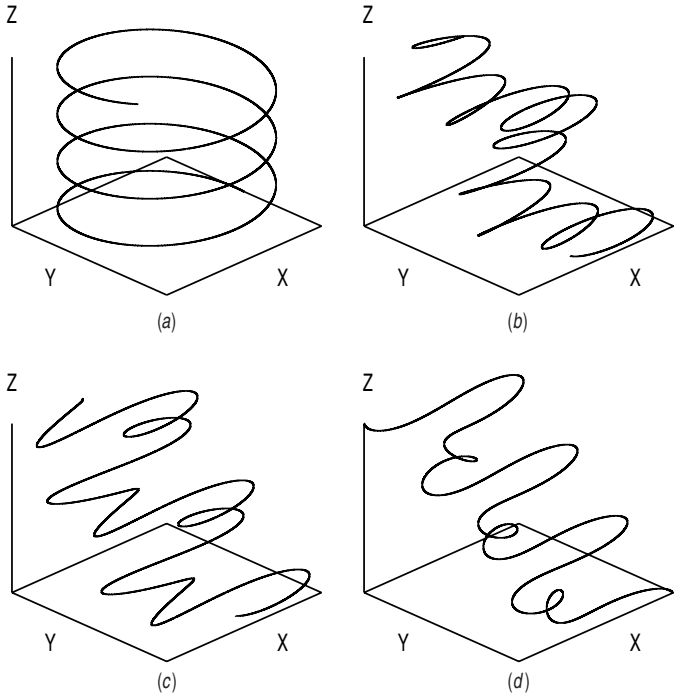


**Figure 4.** Solutions for model I with $\mu = J = 1.0$, $\kappa_0 = 0$ and values of $E$ given by: (*a*) $E = 0.35$, (*b*) $E = 0.40$, (*c*) $E = 0.65$ and (*d*) $E = 1.41$.

## 3. Model Ia: $f(k, \tau) = \frac{1}{2}\kappa^2 + \alpha\tau + \mu$

Let us add a linear term on torsion to equation (2.1). This term can be considered as another constraint on the energy functional given by equation (2.1) for the special case $\kappa_0 = 0$, that is

$$f(k, \tau) = \tfrac{1}{2}\kappa^2 + \alpha\tau + \mu. \tag{3.1}$$

It turns out that this model is also integrable by means of a quadrature, with the effective potential depending again only on the curvature:

$$\tfrac{1}{2}\kappa'^2 + V(\kappa) = E, \tag{3.2}$$

where

$$V(\kappa) = \frac{1}{8}(\kappa^2 - 2\mu)^2 + \frac{1}{8\kappa^2}\left(\alpha\mu - J + \frac{1}{2}\kappa^2\right)^2. \tag{3.3}$$

Before continuing with the analysis of the effective potential, we must mention that this energy minimization problem was already considered by Langer and Singer in [17] and by Ivey and Singer in [18]. In the former, the authors found the solution for both the curvature and torsion in terms of elliptic integrals. In [18] a complete description of the space of closed and quasiperiodic solution curves for this model is given. There remains therefore almost nothing to be said that is not already discussed in these works. Despite this, for the sake of completeness of our work and for visualization purposes, we include this energy functional and we will show some of the solution curves that these authors have not shown explicitly.

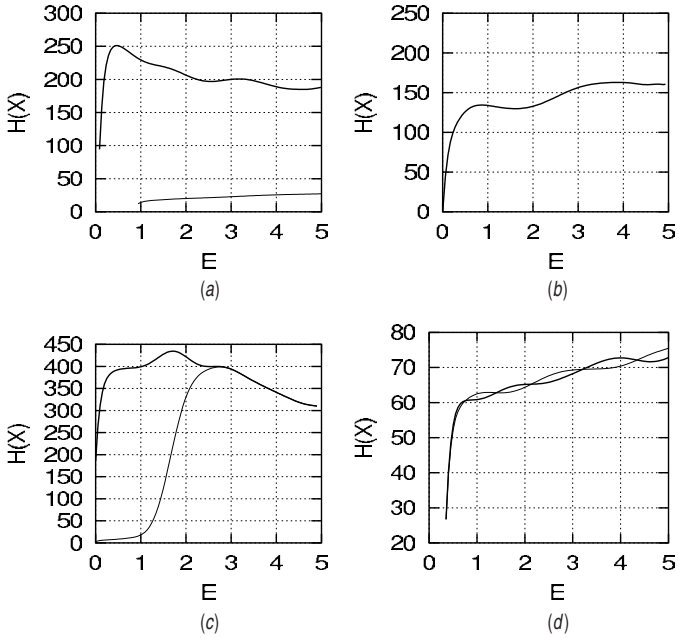


**Figure 5.** Energy $H$ against $E$ for the family of solution curves for the model (2.1) without $\mu$. The values of the remaining parameters for curves in graphs $(a)$, $(b)$ and $(c)$, were given to the same as those used in the effective potential of figure 1 for graphs $(a)$, $(b)$ and $(c)$ respectively. For graph $(d)$ we have used the family of curves found for the case $\kappa_0 = 0$ illustrated in figure 4. Bold lines in this plot correspond to $H$ for the solution curves found for the left branch of $V(\kappa)$ whereas the light lines correspond to $H$ for the solution curves of the right branch of $V(\kappa)$.

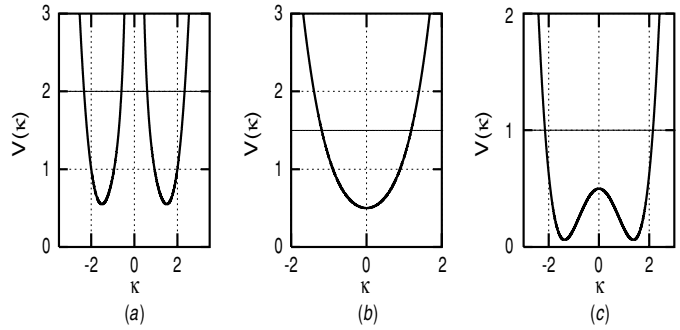


**Figure 6.** Effective potential $V$ for model Ia using the values $(a)$ $\mu = 1\,\alpha = 1\,J = -1$; $(b)$ $\mu = -1\,\alpha = 1\,J = -1$ and $(c)$ $\mu = 1\,\alpha = 1\,J = 1$.

The solutions will now be determined by the set of four parameters $(\mu, \alpha, J, E)$. As in the previous case, $E$ and $J$ are integration constants resulting from the invariance of $H$ under translations and rotations, respectively. As in model I, we can write $\tau$ as a function of $\kappa$ alone:

$$\tau(\kappa) = \frac{\alpha\mu - J}{\kappa^2} + \frac{\alpha}{2}. \tag{3.4}$$

For a combination of parameters such that $\alpha\mu - J \neq 0$ we observe that $V$ has two symmetric branches that extend asymptotically to $\infty$ at $\kappa = 0$, see panel $(a)$ of figure 6 while

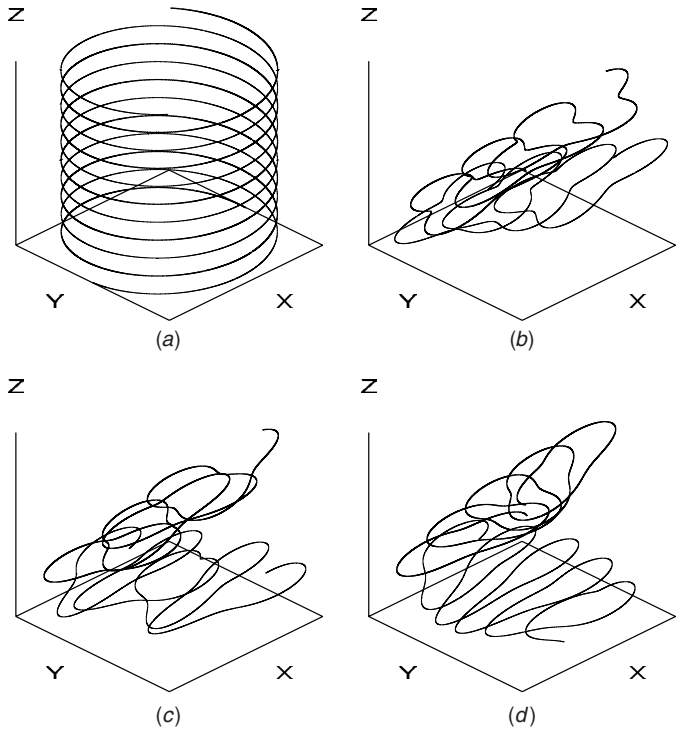


**Figure 7.** Curves from model Ia for $\mu = 1\,\alpha = 1\,J = -1$, with values of $E$ given by: (*a*) $E = 0.5503$, (*b*) $E = 1.0736$, (*c*) $E = 1.5969$ and (*d*) $E = 2.1203$.

for other values of the parameters, $V$ could have one or three critical points, without any asymptotic line. Indeed, the singularity of $V$ at $\kappa = 0$ can be removed if $\alpha\mu - J = 0$.

Consider first the case with $\mu \equiv \frac{J}{\alpha} \leqslant \frac{1}{16}$. Here, $V$ has only one minimum, as shown in panel (*b*) of figure 6. On the other hand, for $\mu = \frac{J}{\alpha} > \frac{1}{16}$ there is a maximum between two minima, panel (*c*) of figure 6. In both cases, $V$ is symmetric under a reflection, $\kappa \to -\kappa$.

In spite of the similarities between the effective potential of models I and Ia, the resulting curves are quite different, and we show in figure 7 solutions for the potential in figure 6(*a*); graph (*a*) shows the helices obtained with $E = V_{\min}$, the minimum of $V$ on both branches. As $E$ grows, the helices turn into more elaborate curves with several loops winding after each other around a circle. We note that these curves resemble the loops obtained in [11], where the functional given in equation (1.5) with area and length constraints was studied. One can say that solution curves found for model Ia are the open partners of those closed curves found in [11]. Likewise, curves obtained from the potential in figures 6(*b*) and 7(*c*) are shown in figures 8 and 9, respectively. In the latter case, the configurations from the left and right branches are identical due to the symmetry of the equations under a reflection $\kappa \to -\kappa$. Thus it is interesting to note that for the last combination of parameters the solution curves have a constant torsion $\tau = \frac{\alpha}{2}$.

As in the previous section, figure 10 shows a plot of the energy $H$ against $E$ for the solution curves obtained. Here as well, curve length was fixed to $L_0$ employed for model I, and none of the curves considered were contained on a plane. We have also integrated out $\mu$ when calculating $H$. Finally, we offer in figure 11 the changes in the geometry of the helix solution for this model when $\mu$ takes values in the interval $(-10, 10)$. We observe that the diameter of

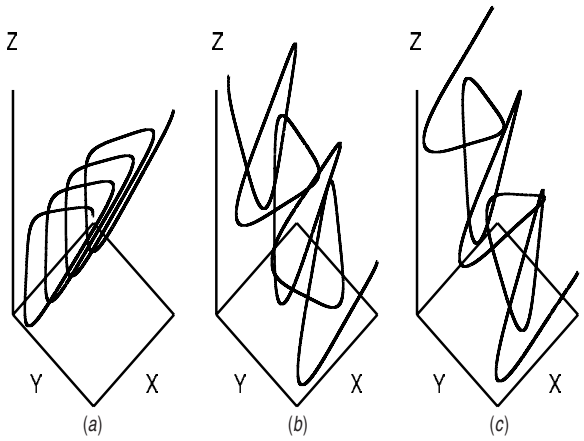


**Figure 8.** Solutions for model Ia with $\mu = -1\,\alpha = 1\,J = -1$, using: (*a*) $E = 1.2037$, (*b*) $E = 3.3148$ and (*c*) $E = 6.8333$.

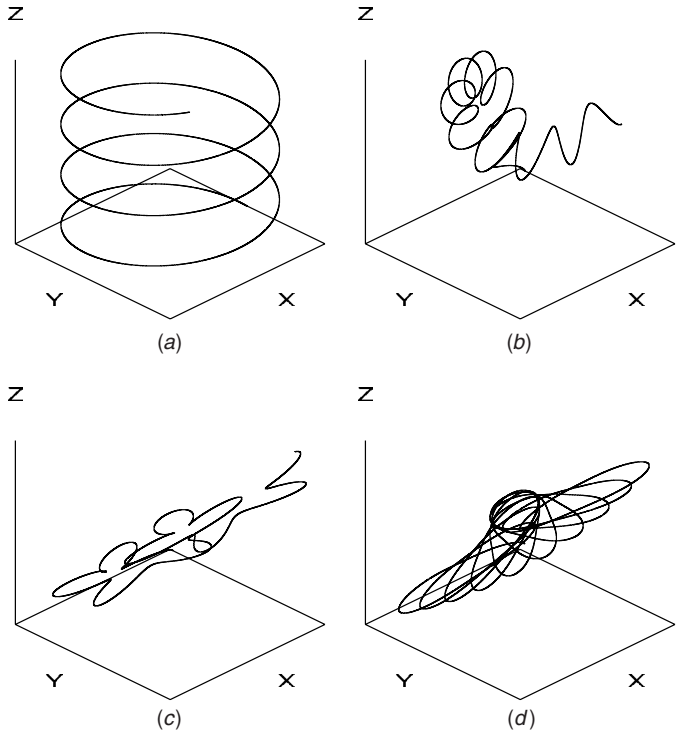


**Figure 9.** Curves for model Ia for $\mu = 1\,\alpha = 1\,J = 1$, with: (*a*) $E = 0.0605$, (*b*) $E = 0.2633$, (*c*) $E = 0.4661$ and (*d*) $E = 0.8041$.

the helix keeps almost constant for large negative values of $\mu$ as was the case found for model I; however, the diameter does not increase as fast as was the case in model I for large positive values of $\mu$.

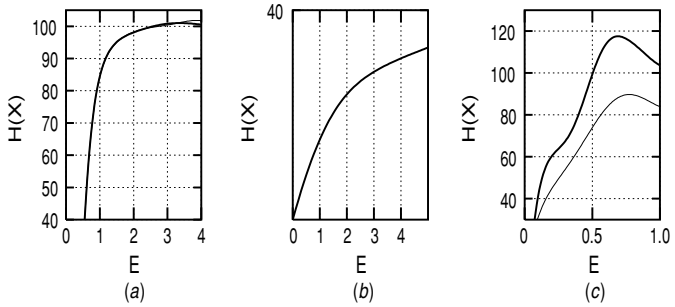


**Figure 10.** Energy $H$ without $\mu$ (see the text for explication) for space curve solutions for the functional (3.1) illustrated in graphs (*a*), (*b*) and (*c*) of figure 6, respectively.

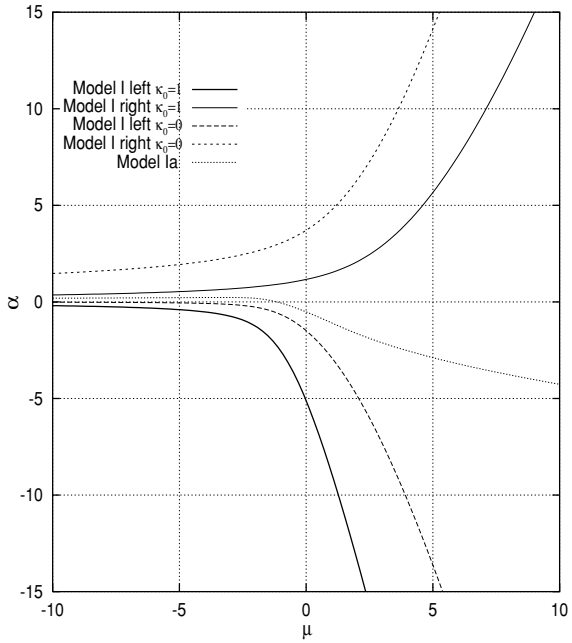


**Figure 11.** Plot of $\alpha \equiv \frac{\kappa}{\tau}$ for helices found at the minimum of either branch (left or right) of the effective potential in model I against $\mu$. The remaining parameters for each model are kept fixed as indicated in the text.

## 4. Model II: $f(\tau) = \frac{1}{2}(\tau - \tau_0)^2 + \mu$

We turn now to a model depending quadratically on torsion alone. This model is more complicated than all the preceding cases considered so far because third order derivatives of **X** are involved and the resulting equations are of sixth order. Surprisingly, however, this model can also be integrated by a quadrature as was demonstrated in [1]. We consider that models II and IIa (to be treated in the next section) are the novel contribution of this work since the analysis of the effective potential has not been reported anywhere as far as we know.

Following again the method developed in [1], it can be shown that, starting with the functional

$$f(\tau) = \tfrac{1}{2}(\tau - \tau_0)^2 + \mu, \tag{4.1}$$

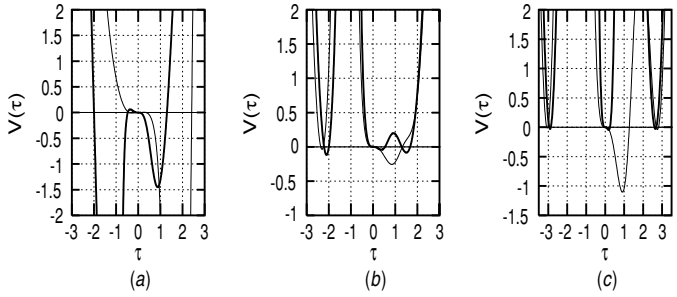


**Figure 12.** The bold (light) lines represent curves for $V(\tau)$ for model II with $\tau_0 = 0$ ($\tau_0 = 1.0$) for fixed parameters $J = 1.0$ and $E = 2$ and with values (*a*) $\mu = -2.0$, (*b*) $\mu = 2.0$ and (*c*) $\mu = 4.0$.

two integration constants $J$ and $E$ can be constructed as follows:

$$J = \frac{1}{2}(\tau - \tau_0)\left(\tau_0^2 - \tau^2 + 2\mu\right) - \tau\left(\frac{\tau'}{\kappa}\right)^2, \tag{4.2}$$

and

$$E = \frac{\kappa^2}{4\tau^2}\left[\left(\frac{\tau'}{\kappa}\right)^2 - f(\tau)\right]^2 + \tau^2\left(\frac{\tau'}{\kappa}\right)^2 + \frac{1}{4}\left(\tau_0^2 - \tau^2 + 2\mu\right)^2. \tag{4.3}$$

We will show now that combining the equations above, $\kappa$ can be expressed solely in terms of $\tau$, which is noteworthy in itself since the torsion then determines the curvature at each point.

Let us start with the special case $\tau_0 = 0$. Solving equation (4.2) for $\frac{\tau'}{\kappa}$ and substituting it in equation (4.3), we obtain

$$\kappa^2(\tau) = 4\tau^4\left[\frac{E + J\tau + \frac{1}{4}\tau^4 - \mu^2}{(J + \tau^3)^2}\right] \tag{4.4}$$

and using equation (4.4) again in equation (4.3), we identify the effective potential $V(\tau)$

$$V(\tau) = \frac{\tau^3}{4}\left[\frac{(4E - 4J\tau + \tau^4 - 4\mu^2)(\tau^3 - 2\mu\tau + 2J)}{(J + \tau^3)^2}\right], \tag{4.5}$$

where we have considered that in this case the quadrature is now written as

$$\tfrac{1}{2}(\tau')^2 + V(\tau) = 0. \tag{4.6}$$

It is important to note that the right-hand side of this quadrature is identically zero, so we need to find the roots of the function $V(\tau)$ in order to determine the boundary conditions or the turning points, $(\tau_{\text{ini}}, \tau_{\text{fin}})$ in order to solve the quadrature for the arc length of the curve.

As long as the expression involved in finding the critical points of $V$, that is $V'(\tau) = 0$, is a ten order polynomial in $\tau$, making it very difficult to follow analytically the properties of $V$ when $\mu$ changes, we will just mention some of the qualitative features of $V(\tau)$ and we will show representative plots generated for different values of $\mu$ while keeping fixed the remaining free parameters of the model.

We note that for all values of the parameters there are always two branches of the effective potential separated by an asymptotic vertical line at $\tau_a = -(J)^{\frac{1}{3}}$. For $\tau \approx \tau_a$ we have that the two branches of $V(\tau)$ go to $-\infty$; while for $\tau \gg |\tau_a|$ (far from the asymptotic line) the two branches of $V$ go to $\infty$ , see bold lines of figure 12. Near the asymptotic line, we emphasize that $V$ changes appreciably for small changes of $\mu$, above all in the interval $-2 < \mu < 2$

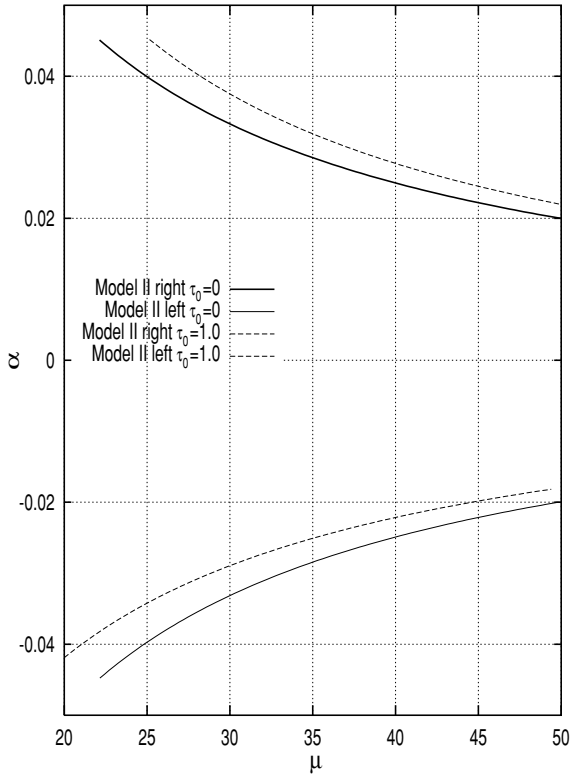


**Figure 13.** Plot of $\alpha \equiv \frac{\kappa}{\tau}$ for helices found at the minimum of either branch (left or right) of the effective potential in model II against $\mu$. The remaining parameters for each model are kept fixed as indicated in the text.

(having fixed $E = 2$ and $J = 1$), as long as the sign of the branches of $V$ are determined by the polynomial $\Delta = 2\mu^3 + \mu^2 - \frac{5}{2}\mu - \frac{5}{4}$ in the limit $\tau - > \tau_a$. $\Delta$ shows up a small maximum followed by a minimum in that interval; out of this interval, for instance for $\tau \gg 2$ then $\Delta - > \infty$ and for $\tau \ll -2$ then $\Delta - > -\infty$.

We have at least two real roots of $V$ apart from the trivial one $\tau = 0$, which does not lead to any interesting solution curve as long as the corresponding curvature is $\kappa = 0$. In that case, every branch is cutting the line $V = 0$ at $\tau \neq 0$ at least one time for all values of the parameters. For positive values of $\mu$, the right branch of the effective potential develops several critical points $\tau_{\text{crit}}$ such that $V'(\tau_{\text{crit}}) = 0$. A typical graph is shown in panel ($c$) and ($b$) of figure 12, where a maximum between two minima can be seen.

It is interesting to note that the wells developed in the two branches of the potential will lead to a cylindrical helix solution when the minimum of the branches touches the horizontal axis $V = 0$ on only one point, see panel ($c$) of figure 12. Of course the value of $\tau_{\text{crit}}$ when this happens depends on $\mu$.

As was done for the helices solutions found in model I, we have followed the form of these helices solutions for model II, both for $\tau_0 = 0$ and $\tau_0 = 1.0$. In figure 13 we have shown the values of $\mu$ for which this event occurs and therefore a helix of a given $\alpha = \frac{\kappa}{\tau}$ can be identified. It should be noted that for model II a large change in $\mu$ implies only a very small change in the geometry of the resulting helices. We observe here the opposite behaviour that was seen to occur for model I, that is, for increasing values of $\mu$ the diameter of the helices

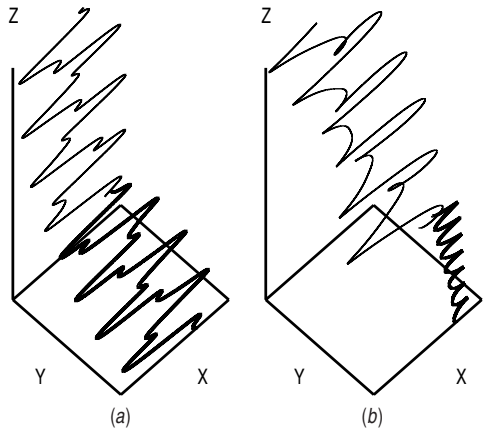


**Figure 14.** (*a*) Curves for model II corresponding to $V$ shown in figure 12(*b*) and with $\mu = 2\ \tau_0 = 0.0\ J = 1.0\ E = 2.0$. and (*b*) Curves for model II with $\mu = 3\ \tau_0 = 1.0\ J = 1.0\ E = 2.0$. In both cases, bold(light) line corresponds to the left(right) well of the effective potential.

are actually decreasing, although this change is at a very small rate. We do not observe any qualitative difference in the behaviour of these $\alpha$ curves against $\mu$ whether $\tau_0$ is zero or not.

In panel (*a*) of figure 14 we show some solution curves for this model.

Let us consider now the case when $\tau_0 \neq 0$. The equations involved for this case are obviously more cumbersome than in the previous case. Fortunately, most of the qualitative features discussed above for the effective potential apply almost without change for the present case irrespective of the value of $\tau_0$. Again, we know that the curvature is determined at each point by the torsion

$$\kappa^2(\tau) = 4\tau^4 \left( \frac{E + J\tau - \frac{1}{2}\tau(\tau - \tau_0)\left(\tau_0^2 - \tau^2 + 2\mu\right) - \frac{1}{4}\left(\tau_0^2 - \tau^2 + 2\mu\right)^2}{\left[\frac{1}{2}(\tau - \tau_0)\left(\tau_0^2 - \tau^2 + 2\mu\right) - J - \tau f(\tau)\right]^2} \right). \tag{4.7}$$

where $f(\tau)$ is given by equation (4.1). Following the convention for the quadrature given in equation (4.6), we find that the effective potential depends again only on $\tau$, although for this case by means of a rather involved relationship:

$$V(\tau) = -\frac{\kappa^2(\tau)}{2\tau}\left[\frac{1}{2}(\tau - \tau_0)\left(\tau_0^2 - \tau^2 + 2\mu\right) - J\right]. \tag{4.8}$$

There are again four parameters to deal with, $(J, E, \mu, \tau_0)$. However, if we fix $\tau_0 = 1$ then we will find almost the same qualitative behaviour for $V(\tau)$ that was found for the case $\tau_0 = 0$ discussed above. For instance, in figure 12 with light line we show $V(\tau)$ for three increasing values of $\mu$ with $\tau_0$, $J$ and $E$ fixed. In all cases, $V$ has two branches. Let us start with graph (*a*): both branches tend asymptotically to $-\infty$ near the asymptotic line at $\tau \approx 1$ and therefore each branch has only one intersection with the axis $V = 0$, so the solution curves will be helices with constant $\kappa$ and $\tau$. In graphs (*b*) both branches tend to $+\infty$ at the new asymptotic line at $\tau \approx -1$ but each of the branches develops its own wells either and they cut the axis $V = 0$ at two points at least, giving place to a solution curve which will be more complex. In panel (*c*) $V$ has three wells; although they look similar to the wells developed by $V$ in the case $\tau = 0$, the curves obtained for each region are very different from each other. Two such curves are shown in panel (*b*) of figure 14 with the bold (light) line corresponding to the left (right) branch of $V$, respectively. Two deformed helices can be recognized, but the deformation is different in each case: for the right well, the circular loops of the original helix

turn into elliptical loops, while for the left well loops of different radii evenly spaced along the helix axis are obtained.

It turns out that the central well of panel (*c*) in figure 12 does not generate any curve at all, because the curvature, equation (4.7), is not real for $\tau$ within this region. This is another rather surprising result, but so far we have not been able to find a fundamental, geometrical reason for such behaviour. The curves obtained for $V$ shown in figure 12(*b*) have essentially the same qualitative properties as before, namely, a deformed elliptical helix corresponds to the left well, and the curvature is not real for the right well.

In figure 13 we offer again the curves for the ratio $\alpha = \frac{\kappa}{\tau}$ against $\mu$ for cylindrical helix solutions. These helices have been formed when both wells of the potential $V(\tau)$ touch the axis $V = 0$ in only one point (within an error of 1.0*e*–3).

## 5. Model IIa: $f(\kappa, \tau) = \frac{1}{2}\tau^2 + \alpha\kappa + \mu$

Although this model is mathematically more complicated than all the models considered so far, it also admits the two basic conserved quantities associated with invariance under translations and rotations. Following, as before [1], one starts with the functional

$$f(\kappa, \tau) = \tfrac{1}{2}\tau^2 + \alpha\kappa + \mu \tag{5.1}$$

and arrives at an expression for constant $E$:

$$E = \frac{\kappa^2}{4\tau^2}\left[\left(\frac{\tau'}{\kappa}\right)^2 - \frac{\tau^2}{2} - \mu + \frac{\alpha\tau^2}{\kappa}\right]^2 + \frac{(\tau^2 - 2\mu)^2}{4} + \tau^2\left(\frac{\tau'}{\kappa}\right)^2, \tag{5.2}$$

and another for constant $J$:

$$J = \frac{\tau}{2}(2\mu - \tau^2) - \left(\tau + \frac{\alpha\kappa}{2\tau}\right)\left(\frac{\tau'}{\kappa}\right)^2 + \frac{\alpha\kappa}{2\tau}\left(\mu + \frac{\tau^2}{2} - \frac{\alpha\tau^2}{\kappa}\right). \tag{5.3}$$

The fact that the term $\frac{\tau'}{\kappa}$ appears squared in both expressions allows us to construct a quadrature, similar to the previous case:

$$\tfrac{1}{2}(\tau')^2 + V(\tau, \kappa) = 0. \tag{5.4}$$

Although $V$ depends now on both $\tau$ and $\kappa$, $\kappa$ can be written in terms of $\tau$, $\kappa = \kappa(\tau)$, and the quadrature can thus be considered as a function of $\tau$ alone, as we will now show.

Eliminating the term $\frac{\tau'}{\kappa}$ in equations (5.3) and (5.2), and after some simplifications, the following polynomial in $\frac{\tau}{\kappa}$ can be written:

$$\begin{aligned}(-4J\tau^3 - \tau^4\alpha^2 - 4E\tau^2 - \tau^6 + 4\mu^2\tau^2)\left(\frac{\tau}{\kappa}\right)^2 \\ + (-4E\alpha\tau - \tau^3\alpha^3 - 4J\alpha\tau^2 + 4\mu^2\alpha\tau - \tau^5\alpha)\left(\frac{\tau}{\kappa}\right) \\ + \left(J^2 + 2J\tau^3 - E\alpha^2 + \tau^6 + \mu^2\alpha^2 + \frac{3}{4}\tau^4\alpha^2\right) = 0.\end{aligned} \tag{5.5}$$

In this way, given a set of values for parameters $(\mu, \alpha, J, E)$, and for a given value of $\tau$, equation (5.5) can be solved for the ratio $\frac{\tau}{\kappa}$ and from here the corresponding value of $\kappa$ can be obtained for the proposed $\tau$.

On the other hand, from equation (5.4) we can identify the corresponding effective potential according to equation (5.4) provided that we translate all other terms to the left side except the one that contains $\tau'$; in doing so we have

$$V(\tau) = -\frac{1}{2}\left(\frac{\tau'}{\kappa}\right)^2\kappa^2 \tag{5.6}$$

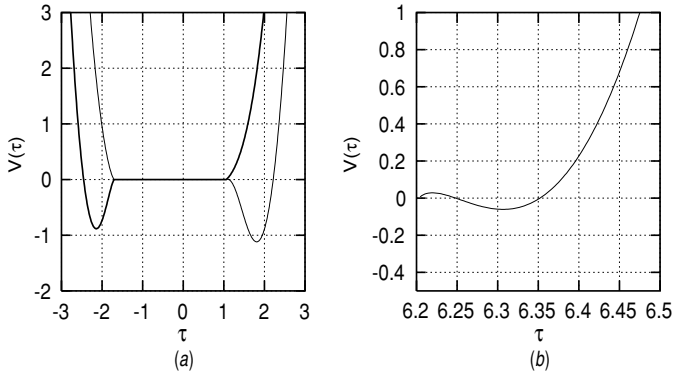


**Figure 15.** Representative graphs of $V$ for model IIa with $(\mu, \alpha, J, E)$ given by: $(a)$ (2.0,1.5, 1.0,2.0) and $(b)$ (20.0,1.5,1.0,2.0). For panel $(b)$ we show only the well of the right branch of the effective potential but it must be emphasized that the global behaviour of the curve is the same as that in panel $(a)$.

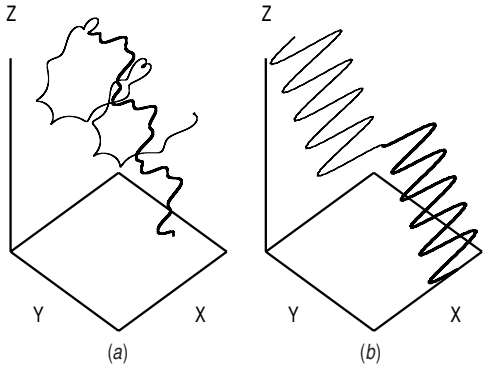


**Figure 16.** Solution curves for model IIa, corresponding to the values of panel $(a)$ in figure 15. Bold(light) line corresponds to the left(right) well of the effective potential.

which can be written by using equation (5.3) again in the form

$$V(\tau) = \frac{1}{4}\left[\frac{4J\left(\frac{\tau}{\kappa}\right) - 4\tau\left(\frac{\tau}{\kappa}\right)\mu + 2\tau^3\left(\frac{\tau}{\kappa}\right) - 2\alpha\mu - \alpha\tau^2 + 2\alpha^2\tau\left(\frac{\tau}{\kappa}\right)}{\left(2\tau\left(\frac{\tau}{\kappa}\right) + \alpha\right)}\right]. \qquad (5.7)$$

Moreover, through the implicit function $\kappa(\tau)$, we can consider that a quadrature in terms of $\tau$ has been obtained: once a pair of values $(\tau, \kappa)$ has been determined, the right-hand side of equation (5.7) gives $V$ implicitly. We have generated a pair of graphs for $V$ in this way; they are shown in figure 15.

It must be emphasized that for most of the parameter space of this model, there are always two real roots for the second order polynomial in $\frac{\tau}{\kappa}$ in equation (5.5), as long as $\tau$ is away from the central region around $\tau = 0$ where no real roots are found. This is why the curve shown in panel $(a)$ of figure 15 appears flat in the central region. We should also mention that each real root of the polynomial gives rise to a curve and to the well that forms each of the two branches of the effective potential.

As was the case when we studied model II, for this model the corresponding solution curves are associated only with the left and right wells, which persist even for large values

of $\mu$ as is shown in panel (*b*) of figure 15. This persistence of the wells prevents us from identifying helices because the wells never rise enough in the plane to touch the axis $V = 0$ in only one point, as was the case in a previous section (at least within an small error around $1.0e{-}3$). We have shown such solution curves in figure 16.

## 6. Conclusions

In this paper we have shown plots of effective potentials and their associated numerical solution curves for a wide class of energy functionals involving both quadratic and linear terms of the curvature and torsion of the curve. Because of the complicated nature of the equations involved for models other than the quadratic-curvature model, for which there is an exact solution known by means of elliptic integrals, in general we have to revert to an analytical treatment especially in the case of quadratic torsion depending functionals. For these cases, we have to content ourselves with a numerical analysis and with a qualitative description of solutions curves as we have done here; and as far as we know, this study is the first of its kind.

It is important to emphasize that the Fortran 77 codes are the main scientific outcome of this work. These codes enable us to get more specific information about the properties of the effective potential and its associated solution curves, allowing us to assemble a showcase of numerical curves as complete as we wish. The authors offer this computational tool (upon request to the authors) for everyone who might be interested in generating an animation of the solutions for his own set of parameters. The full benefits of this computational tool can only be appreciated with the use of an interactive graphic computer.

It could be interesting to consider what the curves would become when we change parameters other than $\mu$. We have not considered all possible cases in the interest of keeping the number of plots of this paper manageable. In a forthcoming paper we will consider the problem of making a classification of solution curves from a geometric point of view. We hope that the view of these new curves and properties may suggest the possibility of taking on use of these energy functionals as approximate models to describe equilibrium states and some mechanical properties of polymer chains [24], as well as the occurrence of supercoiling in the DNA double chain, see [25].

Although it is our opinion that such models can lead to very fruitful results when used as mechanical models, we have not attempted here to describe any particular physical system, nor to study actual properties of complex duplex of supercoiled DNA (see review written by Tamar [26] and references therein). Our main objective has been simply to show more solutions than were previously known. Although we have shown only a very few of them, we have been able to uncover such a huge variety of solutions because of the great advantage that the method of quadratures has compared with other methods.

In fact, the aforementioned applications for the study of polymer chains and DNA, and in particular, their response to shear flow, will be left for a future work. Similarly, a comprehensive investigation of the model quadratic on both the torsion and curvature, equation (1.4), will be presented elsewhere, as the resulting equations cannot be solved by quadratures any longer, and therefore different methods are needed.

We note here that some relevant work may still be done in this field. For example, constructing the Frenet–Serret basis to the case of curves in $N$ dimensions; then will be $N - 1$ scalar curvatures: $\kappa_1$ representing the curvature, $\kappa_2$ the torsion, and so on for $\kappa_{N-1}$. This suggests the possibility to extend the present work to the more general case of energy functionals with quadratic terms of higher curvatures, $\kappa_n^2$. Such cases will be mathematically more complex, but we think that the solution curves could possess confining properties of interest in other dynamical contexts, see e.g. [19].

**Acknowledgments**

GA acknowledges financial support kindly granted from DIP at the UNISON; he thanks ACARUS for the use of computing facilities as well. HV thanks GA for his kind invitation to collaborate on this project.

## Appendix. Numerical implementation

In order to integrate the Frenet–Serret equations (1.2), we need first to solve the quadrature for the model of interest, equations (2.4), (3.2), (4.6) or (5.4), to find $\kappa$ and $\tau$ as functions of $l$. In turn, this implies finding first $l$ from one of these equations, and setting the integration interval for the quadrature. To illustrate the procedure let us take the first case, equation (2.4). Inverting for $l$ we have:

$$l - l_0 = \int_{\kappa_i}^{\kappa_f} \frac{\mathrm{d}\kappa}{\sqrt{2(E - V(\kappa))}}. \tag{A.1}$$

We can fix $l_0 = 0$. The initial and final values of $\kappa$, $\kappa_i$ and $\kappa_f$, correspond to the roots of $V(\kappa) = E$, that is, the values of $\kappa$ for which $\kappa' = 0$ (the 'turning points', if we use the analogy with the particle in a central potential problem). These roots can be computed to a very high accuracy employing Newton's method (see, for instance, [27, 28] for this and the rest of the numerical methods mentioned in this appendix). Once $\kappa_i$ and $\kappa_f$ are known, $l$ can be calculated, but some care is needed to integrate equation (A.1) since the integrand is singular at these points. We have implemented an open Romberg integration imposing an overall accuracy of $\varepsilon = 10^{-7}$. This value of $l$ is used as the interval to integrate the quadrature, equation (2.4), by means of a fourth-order Runge–Kutta scheme, and consistency is ensured by checking that the value of $\kappa$ at the end of the integration is equal to $\kappa_f$ to the same accuracy $\varepsilon$. Equation (2.3) (or the corresponding relation for the studied model) gives the corresponding $\tau$. Finally, these values are used to integrate the Frenet–Serret equations, employing also a fourth order Runge–Kutta integrator.

A word on the initial conditions used to integrate the Frenet–Serret equations is in order. The freedom given to us due to the fact that curvature and torsion determine entirely a curve up to rigid motions can allow us to confine our attention to a helix with symmetry axis parallel to the $z$-axis. Such a curve can be parametrized as:

$$\begin{aligned} x(l) &= a\cos\left(\frac{l}{\sqrt{a^2+b^2}}\right) \\ y(l) &= a\sin\left(\frac{l}{\sqrt{a^2+b^2}}\right) \\ z(l) &= b\left(\frac{l}{\sqrt{a^2+b^2}}\right). \end{aligned} \tag{A.2}$$

The (constant) Frenet–Serret curvatures are:

$$\begin{aligned} \kappa &= \frac{a}{a^2+b^2} \\ \tau &= \frac{b}{a^2+b^2}, \end{aligned} \tag{A.3}$$

which can be inverted to express the helix constants in terms of $\kappa$ and $\tau$:

$$\begin{aligned} a &= \frac{\kappa}{\kappa^2+\tau^2} \\ b &= \frac{\tau}{\kappa^2+\tau^2}. \end{aligned} \tag{A.4}$$

We have used these expressions as initial conditions to integrate the Frenet–Serret equations, since in all models, a solution of the cylindrical helix kind appears. For the purpose of characterizing the geometrical behaviour of the helix when the parameters of the model change, we have also introduced the ratio $\alpha = \frac{\kappa}{\tau}$, which is constant for the cylindrical helix, in fact, $\alpha = -\frac{a}{b}$. Then, we can consider a one-parametric helix in the sense that $a = -\alpha * b$, and therefore that the coefficients appearing in equation (A.2), $(a, a, b)$ transform to $(\alpha, \alpha, 1) * b$; therefore $\alpha$ here describes the radius of the helix and $b$ is merely a scale factor, see figures 11 and 13.

## References


[1] Capovilla R, Chryssomalakos C and Guven J 2002 *J. Phys. A: Math. Gen.* **35** 6571–87
[2] Eisenhart L P 1947 *An Introduction to Differential Geometry* (Princeton, NJ: Princeton University Press)
[3] Kamien R D 2002 *Rev. Mod. Phys.* **74** 953–71
[4] Harris A B, Kamien R D and Lubensky T 1999 *Rev. Mod. Phys.* **71** 1745
[5] Benham C 1979 *Biopolymers* **18** 609–23
[6] Love A E H 1944 *A Treatise on the Mathematical Theory of Elasticity* 4th edn (New York: Dover)
[7] Benham C 1979 *Biopolymers* **22** 2477–95
[8] Wadati M and Tsuru H 1986 *Physica* D **21** 213–26
[9] Antman S S 1995 *A Non Linear Theory of Elasticity* (Berlin: Springer)
[10] Guiaquinta M and Hildebrandt S 1996 *Calculus of Variations* vol 1 (Berlin: Springer)
[11] Arreaga G, Capovilla R, Chryssomalakos C and Guven J 2002 *Phys. Rev.* E **65** 031801
[12] Ou-Yang Z-C, Liu J-X and Xie Y-Z 1999 *Geometric Methods in the Elastic Theory of Membranes in Liquid Crystal Phases* (Singapore: World Scientific)
[13] Bryant R and Griffiths P 1986 *Am. J. Math.* **108** 525
[14] Langer J and Singer D 1984 *J. Lond. Math. Soc.* **30** 512–20
[15] Safran S A 1994 *Statistical Physics of Surfaces, Interfaces and Membranes* (Reading, MA: Addison-Wesley)
[16] Nizette M and Goriely A 1999 *J. Math. Phys.* **40** 2830–66
[17] Langer J and Singer D 1996 *SIAM Rev.* **38** 605–18
[18] Ivey T A and Singer D A 1999 *Preprint* math.DG./9901131
[19] Arreaga G, Capovilla R and Guven J 2001 *Class. Quantum Grav.* **18** 5065–83
[20] Record M, Mazur S, Melancon P, Roe J, Shaner S and Unger L 1981 *Annu. Rev. Biochem.* **50** 997
[21] Kamien R D, Lubensky T C, Nelson P and O'Hern C S 1997 *Europhys. Lett.* **38** 237–42
[22] Marko J F 1997 *Europhys. Lett.* **38** 183–8
[23] Bouchiat C and Mezard M 1998 *Phys. Rev. Lett.* **80** 1556–9
[24] Goldstein R E and Langer S A 1995 *Phys. Rev. Lett.* **75** 1094–7
[25] Olson W K, Sarma S H and Sundaralingan M 1987 *Proc. fifth conversation in the discipline biomolecular stereodynamics* vol 3 (New York: State University New York)
[26] Schlick T 1995 *Curr. Opin. Struc. Biol.* **5** 245–62
[27] Abramowitz M and Stegun I A 1965 *Handbook of Mathematical Functions* (New York: Dover)
[28] Press W H, Teukolsky S A, Vetterling W T and Flannery B P 1999 *Numerical Recipes* 2nd edn (Cambridge: Cambridge University Press)